Optica Applicata, Vol. LV, No. 1, 2025
DOI: 10.37190/oa/196289

Based on fiber sensor network rail transit IoT monitoring system

ZHAO LIU[1], YIFANG WANG[1,*], YINGJUAN HOU[2], CHUNRONG YU[2]

[1]Department of Computer Science and Engineering, Cangzhou Normal University, Cangzhou, 061600, Hebei, China

[2]China Helicopter Research and Development Institute, Tianjin, 300011, China

[*]Corresponding author: wangyifangczsy@sina.com

In the process of train operation, the status information directly reflects the degree of safety of the operation. Online health monitoring and completion of train status assessment are important signs of train intelligent control. To obtain the stress field distribution of the support position (bearing area) of the train, proposed a EMU health monitoring and intelligent state assessment system based on fiber sensing internet of things (FS-IoT). The system adopts the method of combining multiple sensitized FBG sensors into a sensing network to obtain the stress field distribution at the measured location. When the train is faulty or the external environment affects the train's operation, the stress field and vibration field on the train's motion components will change significantly. Obtain real-time physical field information of sensitive locations through the FBG sensor array, which can realize online monitoring of train status. A distributed combinatorial optimization algorithm based on FS-IoT was designed, and the weight distribution of FBG test data at different locations on the inversion results was analyzed based on data mining. In the sensitization FBG testing experiment, under the same stress conditions, the sensitivity increased from 12.440 to 49.935 pm/kN, and had good linearity. In dynamic testing, when the test carriage passes through the rail connection, there will be significant fluctuations in the center wavelength of the FBG, with a maximum wavelength offset of 2530.2 pm. The peak-to-peak values of the two test data are basically the same, indicating that stress changes can be inverted by the peak position. Finally, a train state inversion model based on FBG sensing network and a system framework for intelligent state evaluation are presented, providing new design ideas for train state monitoring.

Keywords: fiber sensing internet of things (FS-IoT), fiber Bragg grating (FBG), health monitoring, state assessment, electric multiple units (EMU).

1. Introduction

Railway is an important means of transportation between cities, and the safe operation and reasonable dispatch of trains have become the current research hotspots of intelligent transportation [1]. It includes two aspects: first, monitoring and maintenance of

railway infrastructure; second, monitoring and feedback control of train status. By using sensors reasonably, the health status of railway tracks and trains can be predicted, so that potential problems can be detected early and serious traffic accidents can be avoided. The state of the train is analyzed through the test data, and the intelligent control of the train is realized according to the mathematical model of the state risk assessment, so as to ensure the optimal efficiency in a healthy state.

In recent years, optical fiber sensing technology has been widely used in condition monitoring in various industrial fields [2], especially in the field of structural health monitoring. In the early days, due to the principle of technology and cost, it was mainly used in aircraft health monitoring. With the development of processing technology, its cost has been greatly reduced, so it has gradually been applied to the monitoring field of important transportation facilities such as railways and highways. In particular, distributed [3-5] and quasi-distributed [6-10] optical fiber sensors have become very common for health monitoring of large infrastructures (such as pipelines, tunnels, and bridges).

Compared with traditional electronic sensors, optical fiber sensing technology has many advantages, such as the ability to resist electromagnetic interference, and is suitable for harsh environments (such as strong vibration and static electricity) [11]. It also has low invasiveness, huge multiplexing capabilities, *etc*. According to the classification of the structure, it can be divided into two categories: the first category is distributed optical fiber sensing technology, including Raman scattering [12], Brillouin scattering [13] and Rayleigh test methods for scattering, *etc*. In this type of optical fiber sensing system, the optical fiber is the sensing element. The Raman, Brillouin, Rayleigh and other scattered signals acquired by reflection at different positions of the optical fiber become the information source of the physical field state at that position, and then the state information is obtained by demodulating the echo spectrum. The second category is quasi-distributed optical fiber sensing technology, which mainly uses various types of optical fiber grating sensors to complete data acquisition and analysis. The basic principle is to form an echo signal with a specific center wavelength by engraving a grating on an optical fiber. Monitor the state of the physical field at a fixed location. Both methods have their own characteristics. For distributed optical fiber sensing technology, because the location of the test point only depends on the spectral resolution capability of the system on the time axis, a large amount of point data can be obtained, which is very suitable for large-scale and long-distance condition monitoring. Its disadvantages are low test accuracy, low signal-to-noise ratio, and high requirements for system data processing capabilities. For the quasi-distributed optical fiber sensing technology, using the reflection characteristics of FBG, it has high accuracy, high signal-to-noise ratio, and good stability. Its disadvantage is that it only supports point testing, and the number of test points on a single fiber is limited by the modulation band.

FILOGRANO *et al*. [14] announced that it will simultaneously apply FBG and RDTS to the monitoring of rail conditions, and has obtained an effective prediction of landslide hazards. AL-TARAWNEH *et al*. [15,16] used FBG for load monitoring on flexible

road surfaces, and constructed a functional relationship between stress transfer and wavelength shift by designing a new type of sensor package. ZHANG *et al*. [17] applies distributed optical fiber to multiple existing railway tracks and obtains a large amount of actual test data, providing risk assessment for railway tunnel safety monitoring. LIU *et al*. [18-20] sampled FBG to complete the stress field detection of free-form surfaces, with a testing accuracy of 15 pm/με, and also achieved three-dimensional stress field reconstruction under static conditions. In addition, there are many related literature reports, but in summary, we can find that most of the literature research focuses on the train track, because the track monitoring has good stability and the effect of monitoring the environmental impact is obvious. However, the literature on monitoring the running status of the train itself is still mostly focused on the use of traditional electronic sensing equipment.

This article applies fiber optic sensing internet of things (IoT) to the monitoring of rail trains and designs an enhanced FBG sensor to address the impact of strong vibration signals on stress field testing during train operation. Intended to obtain real-time status data of rail trains and provide assurance for safe operation.

2. System design

The fiber optic IoT mainly consists of a perception layer, a network layer, and an application layer. Among them, the perception layer is a fiber optic sensing network tightly attached near the mixed wheel position of the track train. The network layer includes data acquisition modules, data flow control modules, and optical switches used for testing signal transmission. The application layer is the terminal control end, including monitoring platforms, traffic command centers, *etc*.

The fiber optic sensing IoT is composed of tunable laser, optical isolator, fiber coupler, demodulator, fiber grating sensor, *etc*. The system structure is shown in Fig. 1.

The modulated light source sweeps the light of the incident fiber. The incident light enters the fiber sensor network through the fiber coupler and reaches the position of the strain sensing module (FBG sensor), and loads the strain information at the corresponding position into the wavelength change information. Fix the FBG on the sensi-

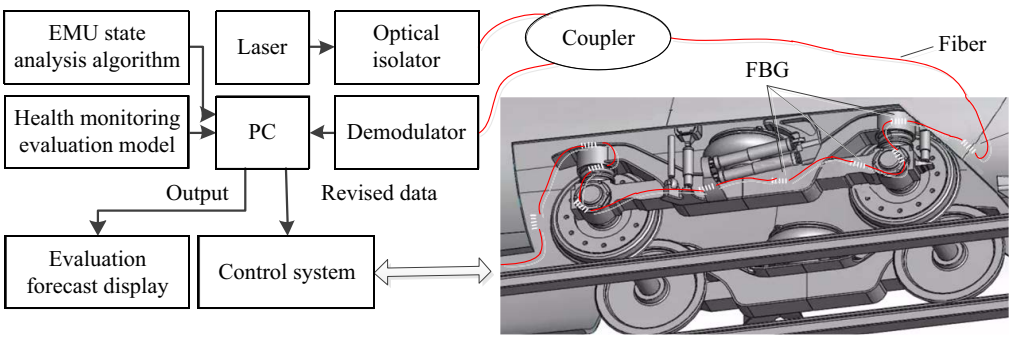

Fig. 1. Schematic diagram of the FBG array sensing network system.

tive position of the train wheel set, to obtain real-time data of the status information of the train to be measured, so as to realize risk assessment for train operation health. When the train is disturbed during operation, or the vibration state of the train changes due to external factors such as the track, the stress field and vibration field signals of the key parts of the train will also change accordingly. As long as the signal feature classification of different safety issues is completed in advance, the risk assessment and online adjustment can be completed through the monitoring data of the FBG sensing array when the train is running. Use the real-time health monitoring data of this system to achieve intelligent monitoring and control of train operation status and realize the intelligentization of railway traffic.

3. Train status monitoring model

3.1. FBG principle

When the train is in motion, it will rub against the rail. First, the pressure will cause the deformation of the wheels and supporting parts, and the second is the periodic vibration when passing through the rails. These two physical quantities can reflect the state characteristics of the moving parts of the train, so as to achieve the purpose of health monitoring through these state characteristics. The moving part of the train will be deformed by squeezing, *etc*., which will cause the corresponding deformation of the FBG and shift the center wavelength λ_B of the echo. Using the linear relationship between wavelength and strain, the stress distribution of each sensitive position on the train can be obtained. Assuming that the monitoring environment temperature remains unchanged, the center wavelength λ_B is only related to the effective refractive index n_{eff} and the grating period Λ, and the following relationship is satisfied [21]:

$$\lambda_B = 2n_{eff}\Lambda \tag{1}$$

Among them, n_{eff} is the core refractive index and Λ is the FBG period.

Due to the gradual temperature variation signal during train operation, using a high pass filter to filter the initial data can eliminate the influence of FBG echo wavelength on temperature [19]. When the influence of temperature changes is not considered, according to the strain monitoring, the function relationship between the change of the center wavelength and the strain is:

$$\Delta\lambda_B = \lambda_B(1 - P_\varepsilon)\varepsilon \tag{2}$$

Among them, λ_B is the center wavelength of the FBG echo, P_ε is the elasticity coefficient, and ε is the amount of strain.

3.2. Optimized FBG structure design

To solve the interference problem of vibration noise on stress field testing during train operation, a FBG packaging structure capable of differential data processing was designed. There are many sensitization packaging designs for stress sensing in existing

literature, including sensitization bridge structures. However, due to the special application scenario of this system and its strong vibration signal, an additional hollow sandwich structure design has been added. The main innovation of this design is to significantly reduce surface tension transmission through the non-adhesive form of FBG sensors and test surfaces, while the hollow structure can effectively maintain the extraction of vibration signals. This design is equivalent to setting stress and vibration as two independent variables, and then the response parameters corresponding to the two packaging structures are completely different, thus achieving the goal of simultaneous solution.

FBG1 adopts a bridge structure to improve stress response, and due to its close proximity to the testing position, vibration noise will also be superimposed on the echo signal of FBG1. The structure of FBG2 is hollow, and there is no adhesive between FBG2 and the test surface. It is also fixed in the testing position, the stress effect is significantly weakened due to its hollow shape. On the contrary, its vibration response is more pronounced. Therefore, differentiating the center wavelength offset data of FBG2 from the data of FBG1 can effectively suppress the interference of vibration noise on stress field testing.

During the operation of rail trains, vibration noise causes the greatest interference to stress field testing. So this article designs an FBG packaging structure with vibration noise suppression, as shown in Fig. 2.

As shown in Fig. 2, the new FBG sensor consists of two parts. The left half of the FBG sensor is glued and solidified at both ends to set the pre-stress. Aluminum foil material is used in the FBG grid area to improve strain conduction efficiency, and adhesive fixation is completed to enhance strain sensitivity. And the two ends of the FBG sensor in the right half are not glued, that is, no pre-stress is set, which greatly reduces the influence of the stress field on the sensor. However, since both FBGs will receive the same vibration noise, using the signal on the right side as the vibration noise source can significantly improve the strain monitoring accuracy of the left FBG sensor.

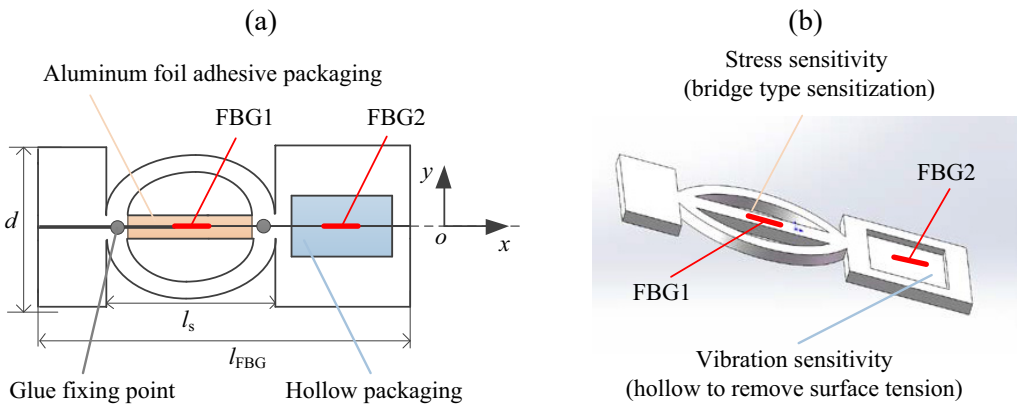

Fig. 2. Schematic diagram of the packaging structure of the optimized FBG. (a) Flat structure, and (b) 3D structure.

For FBG1, due to the structural design of adhesive fixation and aluminum foil packaging, the strain response of the testing position will be well tested. In addition, the vibration noise during train movement, combined with Eq. (2), it is

$$\Delta\lambda_{B1} = \lambda_{B1}(1 - P_\varepsilon)\left[\varepsilon_{strain} + \varepsilon_{noise}(t)\right] \tag{3}$$

Among them, ε_{strain} represents the strain value of the area to be monitored, $\varepsilon_{noise}(t)$ represents the strain value caused by train vibration in motion, and t represents time.

For FBG2, due to the lack of adhesive fixation and sealing treatment on the sensitive areas of FBG, the influence of stress on it is very small. The central area is a hollow packaging structure, so the stress at the testing structure location has almost no effect on it, while the strain values caused by vibration noise still exist. Therefore, the wavelength change value of its echo is

$$\Delta\lambda_{B2} = \lambda_{B2}(1 - P_\varepsilon)\varepsilon_{noise}(t) \tag{4}$$

Combining Eqs. (3) and (4) yields

$$\varepsilon_{strain} = \frac{1}{1 - P_\varepsilon}\left(\frac{\Delta\lambda_{B1}}{\lambda_{B1}} - \frac{\Delta\lambda_{B2}}{\lambda_{B2}}\right) \tag{5}$$

The above theoretical derivation verifies that the optimized FBG structure design can effectively suppress the influence of train vibration noise on structural stress testing.

3.3. Monitoring model

The wavelength shift caused by stress and vibration can be written as

$$\Delta\lambda_B = \Delta\lambda_{B1} + \Delta\lambda_{B2} = k_\varepsilon \varepsilon_{strain} + k_V \varepsilon_{vibration} \tag{6}$$

Among them, k_ε is the strain response coefficient, and k_V is the vibration response coefficient. Due to the different packaging structure designs of FBG, there is a significant difference between k_ε and k_V. The relationship between two wavelength offsets is

$$\begin{bmatrix}\Delta\lambda_{B1}\\ \Delta\lambda_{B2}\end{bmatrix} = \begin{bmatrix}k_\varepsilon\\ k_V\end{bmatrix}\begin{bmatrix}\Delta\varepsilon\\ \Delta V\end{bmatrix} \tag{7}$$

Among them, $\Delta\lambda_{B1}$ and $\Delta\lambda_{B2}$ represent the echo wavelengths collected by two different packaged FBG sensors, respectively. After differential processing of the two signals, the proportion of stress and vibration offset at the final wavelength can be calculated, thus completing the removal of vibration noise.

The stress data after removing vibration interference can be used for inversion of positional deformation. It will cause the FBG to produce the corresponding set of digital model standard points of the stress field to be tested as $U(x, y, z)$, then when the external environment is changing, the actual test data set is $U'(x, y, z)$. In order to ensure

that the deformation caused by the state change during the train running process of the train status parameters does not cause the out-of-tolerance phenomenon, it is necessary to obtain the deviation set $\Delta U(x, y, z)$ between the safe operating parameters and optimal operating parameters, which passes through the strain field inversion. There are

$$\begin{cases} U'(x, y, z) = U(x, y, z) - \Delta U(x, y, z) \\ \Delta U(x, y, z) = f(\varepsilon) U(x, y, z) \end{cases} \tag{8}$$

Finally, the coordinates of the actual standard point can be calculated as

$$U'(x, y, z) = \left[1 - f(\varepsilon)\right] U(x, y, z) \tag{9}$$

Among them, $f(\varepsilon)$ is a function of strain field. In order to obtain its accurate expression, it can be obtained by decomposing the three-coordinate value of any point.

4. Simulation analysis

We conducted simulation analysis on the strain field of the wheel axle position during train motion by ANSYS. The simulation material is steel, with an elastic modulus of 2.2×10^5 MPa, a density of 7780 kg/m^3, a Poisson's ratio of 0.286, and a cross-sectional area of 60 cm^2. The simulation results are shown in Fig. 3.

As shown in Fig. 3(a), when the test carriage is 30 tons, the maximum strain value in the FBG sensor is 5.0485×10^{-8}. As shown in Fig. 3(b), when the test carriage is 60 tons, the maximum strain value in the FBG sensor is 7.9679×10^{-8}. The minimum strain values in both states are 5.7143×10^{-9}, indicating that detectable strain is only generated in some sensitive locations, which are also the deployment positions of FBG sensors. In Fig. 3, it can be seen that the strain distribution at the position of the train bearings exhibits a radial diffusion pattern centered on the point of application,

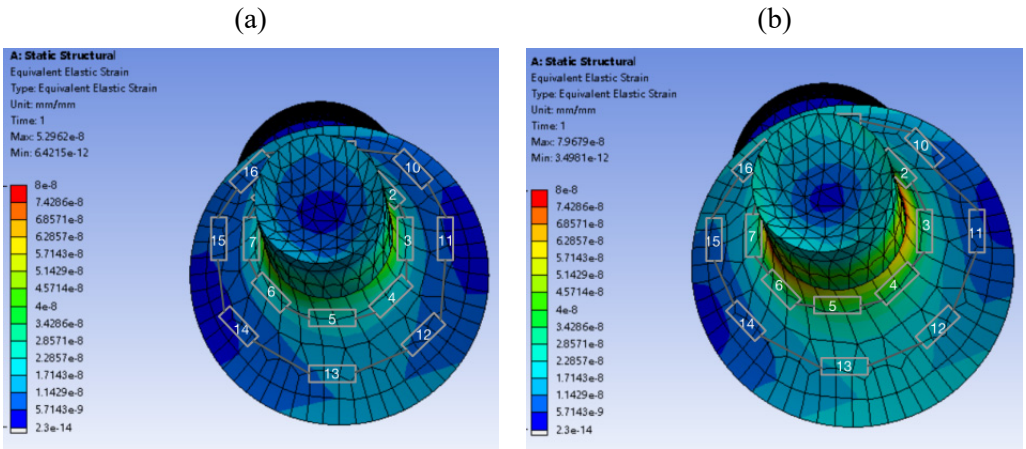

Fig. 3. Stress field distribution of trains under different load conditions. (a) 30 tons, and (b) 60 tons.

and the deformation gradually decreases from the center position towards the bearing center. The stress field regions on both sides will show differences at different positions, and there is a stress field extension between the train bearings and the rails. But the main deformation is concentrated on the contact surface between the bearing and the wheel. The stress field distribution of this test area can be obtained at the 16 positions marked in the simulation diagram, and the contact position with the rail can be analyzed at positions 9–16. Comparing Figs. 3(a) and (b), the strain field distribution of the bearing is not uniform, and the center stress point is offset in the direction perpendicular to the rail. Similarly, if the stress field distribution in the area is quantitatively analyzed, it can reflect the operating status of the train and provide data support for safe operation.

5. Experiment

5.1. Stress sensitivity of optimized FBG

The sensitization effect of the FBG packaging structure designed in this article was tested. During the test, the force application positions were located directly above the test point and offset by 30cm from the test point. The purpose of using these two force application positions was to compare and analyze the difference between the positive position force and the lateral interference force. Because the train wheels are designed side by side, reducing stress interference through packaging during testing can more effectively invert the track state.

The test was conducted using an incremental force application method, with a force range of [0 kN, 30 kN]. The wavelength shift was recorded every 1 kN change, and the test results of the sensitized FBG (S-FBG, sensitive FBG) in this study were compared with those of the traditional FBG (T-FBG, traditional FBG). The results are shown in Fig. 4.

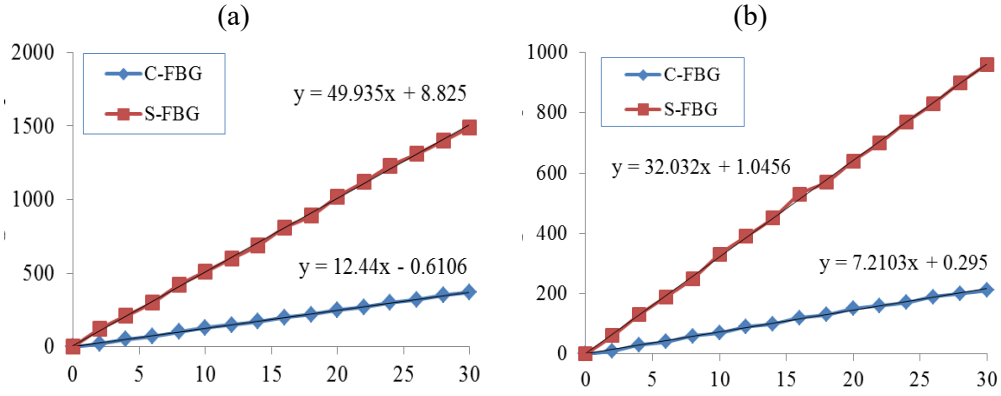

Fig. 4. Stress field distribution at two typical locations. (a) Directly below the wheel axle, and (b) offset 30 cm from the wheel axle position.

As shown in Fig. 4(a), directly above the contact position between the wheel and the rail, the sensitivity of S-FBG is 49.935 pm/kN, and the sensitivity of C-FBG is 12.440 pm/kN. The wavelength responsivity of S-FBG is significantly better than that of C-FBG. The linearity of the two within the testing range of [30 kN, 60 kN] is relatively good, which means that the strain values at the testing location can be calculated through linear fitting. As shown in Fig. 4(b), comparing different test positions, it can be seen that the wavelength shift caused by the same load has significantly decreased, but its linearity is still good. Due to a 30 cm offset in the testing position, the corresponding strain decreases, resulting in an overall decrease in the wavelength offset value. The sensitivity of S-FBG is 32.032 pm/kN, and the sensitivity of C-FBG is 7.210 pm/kN. The wavelength responsivity of S-FBG is still better than that of C-FBG.

5.2. Dynamic response analysis

Measure the internal transmission rail of a certain section, and use an independent single section mining carriage to simulate the process of track compression under stress load. Set the speed to 10 m/s and fill the carriage with sand to achieve an equivalent stress of 10 kN. The response to stress changes within a range of 100 m at the testing point was tested, with a sampling frequency of 1.0 kHz. The wavelength change curve is shown in Fig. 5.

As shown in Fig. 5, with the increase of time, when the test carriage passes through the rail connection, the center wavelength of the FBG will show significant fluctuations, with a maximum wavelength offset of 2530.2 pm. The peak-to-peak values of the two test data are basically the same, indicating that stress changes can be inverted by the peak position. As the carriage moves away from its normal position, the wavelength gradually returns to its initial state value. Due to the short duration of the two tests and negligible temperature changes, static temperature drift compensation can meet the design requirements. The response value of the positive position increased by about 30% compared to the static state. Analysis suggests that this is caused by the vibration generated by the load movement, which oscillates the test wavelength of the FBG. This

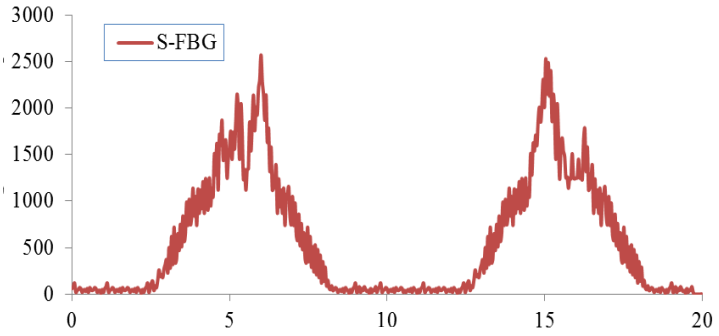

Fig. 5. Stress dynamic response curve directly above the wheel axle within 20 s.

problem can be suppressed by differential tuning of two or more sets of test data to suppress vibration interference.

In the actual testing process, whether it is train braking, foreign objects on the rails, abnormal speed, *etc*., it will cause changes in the distribution of response wavelengths at the testing position. In the test, we analyzed the test data under different speed conditions and found that the faster the speed, the more forward the axial direction of the stress diffusion line. Due to space limitations, no specific calculation has been provided for its quantitative relationship, but its trend can be used for indirect analysis of velocity anomalies. Similarly, placing foreign objects such as iron nails on the railway track will increase the peak-to-peak wavelength at that location, and this increase can also be applied to auxiliary monitoring of abnormal states.

5.3. Distribution design for EMU

The FUXING EMU measured the moving parts during the assembly stage. Suppose the plane test points are respectively P_{p1}, …, P_{pn}, the regular surface test points are

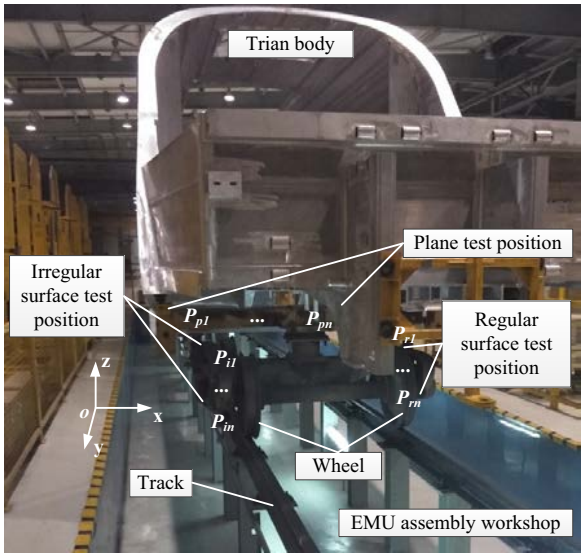

Fig. 6. Design of monitoring position of FBGs sensing array on EMU.

T a b l e 1. Data mapping relationship.

Types	Axiality of FBG	Representational relationship
P_{p1}, …, P_{pn}	*x*-axis, *y*-axis, *z*-axis	Status information on the three axes in the EMU Cartesian coordinate system
P_{r1}, …, P_{rn}	Angle α in the plane formed by the *y*-axis and *z*-axis	Status information of wheel rotation posture
P_{i1}, …, P_{in}	Other directions used to supplement missing	Parameter weight compensation of status information

respectively $P_{r1}, \ldots, P_{rn}$, and the irregular surface test points are respectively $P_{i1}, \ldots, P_{in}$. The distribution of test points is shown in Fig. 6.

The main physical field characterization relationships corresponding to different test points will be given below. Through different mapping relationships, a large amount of test data can be classified, and data mining with predictable weights can be completed, in order to provide quantitative analysis data support for EMU operating status evaluation. The corresponding relationship was shown in Table 1.

5.4. Intelligent state assessment for EMU

Intelligent status assessment is mainly for real-time monitoring of common failures during train operation, and emergency measures are given according to the type of failure. The main types of failures are: brake failure, tailpipe not hoisted failure, door or window not closed, *etc*. In addition, it also includes possible hazards in the operating environment, such as derailment of the train when the turning radius is small and the speed is high.

In view of the above existing fault classification, according to the characteristics of the mathematical model corresponding to the physical process, the following intelligent state assessment evolution relationship diagram is given, as shown in Fig. 7.

According to the logical relationship shown in Fig. 7, the test data collected by the system and the parameters calculated above are substituted into the Intelligent State Assessment system for EMU. The real-time data obtained by the FBG sensing array

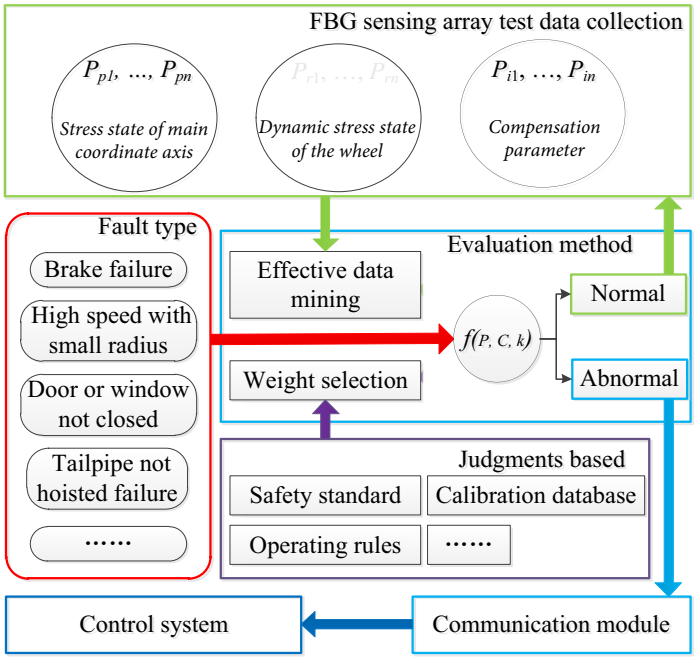

Fig. 7. Intelligent state assessment system for EMU.

can be used to complete online monitoring of the EMU status, and the EMU operating status health evaluation level can be given according to the operating rules and driving conditions, so as to realize the intelligent monitoring and correction of the EMU operation. The system can be applied to various train models currently in operation, and the data of a single train can also be interconnected through a wireless network to realize intelligent traffic management and control of multi-station networking.

6. Conclusions

In this research, the authors developed an EMU health monitoring and intelligent state assessment system to monitor the status information of EMU by Bragg grating sensors network and the distributed combination optimization algorithm. The conclusions of this paper are:

1) The system can effectively obtain the status parameter information of the EMU through the FBG sensor network in real time.

2) An optimized FBG packaging structure is designed that is stress sensitive but insensitive to vibration noise.

3) The three surface structures can completely characterize the main surface distribution of the train moving position, and the FBG test data contribution weight coefficients can be obtained according to the different surface characteristics.

4) The optimized FBG sensor has higher sensitivity and can obtain real-time status information of the train in dynamic testing results.

5) The intelligent state assessment system for EMU is constructed to realize closed -loop feedback of monitoring and control.

Overall, the system can obtain real-time train operation status parameters by monitoring the stress field. This study provides new ideas for the control of intelligent high -speed trains.

Acknowledgment
This research is supported by Cangzhou Natural Science Foundation Project (No. 2210001014D).

References

[1] KARACOCUK G., HÖFLINGER F., ZHANG R., REINDL L.M., LAUFER B., MÖLLER K., *Inertial sensor-based respiration analysis*, IEEE Transactions on Instrumentation and Measurement **68**(11), 2019: 4268-4275. https://doi.org/10.1109/TIM.2018.2889363

[2] OH H.-S., SIM J., *Interface debonding failure in beams strengthened with externally bonded GFRP*, Composite Interfaces **11**(1), 2004: 25-42. https://doi.org/10.1163/156855404322681037

[3] HODGE V.J., O'KEEFE S., WEEKS M., MOULDS A., *Wireless sensor networks for condition monitoring in the railway industry: A survey*, IEEE Transactions on Intelligent Transportation Systems **16**(3), 2015: 1088-1106. https://doi.org/10.1109/TITS.2014.2366512

[4] ZHANG L., HAAS C., TIGHE S.L., *Evaluating weigh-in-motion sensing technology for traffic data collection*, [In] *Proceedings of Annual Conference of the Transportation Association of Canada*, Saskatoon, Saskatchewan, Canada, 2007: 1-17.

[5] Mihailov S.J., *Fiber Bragg grating sensors for harsh environments*, Sensors **12**(2), 2012: 1898-1918. https://doi.org/10.3390/s120201898
[6] Muanenda Y., Faralli S., Oton C.J., Di Pasquale F., *Dynamic phase extraction in a modulated double-pulse ϕ-OTDR sensor using a stable homodyne demodulation in direct detection*, Optics Express **26**(2), 2018: 687-701. https://doi.org/10.1364/OE.26.000687
[7] Issatayeva A., Beisenova A., Tosi D., Molardi C., *Fiber-optic based smart textiles for real-time monitoring of breathing rate*, Sensors **20**(12), 2020: 3408. https://doi.org/10.3390/s20123408
[8] De Tommasi F., Massaroni C., Caponero M.A., Carassiti M., Schena E., Presti D.L., *FBG-based mattress for heart rate monitoring in different breathing conditions*, IEEE Sensors Journal **23**(13), 2023: 14114-14122. https://doi.org/10.1109/JSEN.2023.3275323
[9] Kikuchi K., Naito T., Okoshi T., *Measurement of Raman scattering in single-mode optical fiber by optical time-domain reflectometry*, IEEE Journal of Quantum Electronics **24**(10), 1988: 1973-1975. https://doi.org/10.1109/3.8529
[10] Kong L.Q., Wu Y.H., Pang Z.G., Zhao Y.J., Dong L.Q., Liu M., Hui M., Wang W.J., Guo Y., Wang X.T., *Measurement of heart rate based on ballistocardiography*, Chinese Journal of Lasers **47**(2), 2020: 0207042. https://doi.org/10.3788/CJL202047.0207042
[11] Majumder M., Gangopadhyay T.K., Chakraborty A.K., Dasgupta K., Bhattacharya D.K., *Fibre Bragg gratings in structural health monitoring—Present status and applications*, Sensors and Actuators A: Physical **147**(1), 2008: 150-164. https://doi.org/10.1016/j.sna.2008.04.008
[12] Burnos P., Gajda J., *Thermal property analysis of axle load sensors for weighing vehicles in weigh -in-motion system*, Sensors **16**(12), 2016: 2143. https://doi.org/10.3390/s16122143
[13] Bernal E., Spiryagin M., Cole C., *Onboard condition monitoring sensors, systems and techniques for freight railway vehicles: A review*, IEEE Sensors Journal **19**(1), 2019: 4-24. https://doi.org/10.1109/JSEN.2018.2875160
[14] Filograno M.L., Corredera P., Rodríguez-Plaza M., Andrés-Alguacil A., González-Herráez M., *Wheel flat detection in high-speed railway systems using fiber Bragg gratings*, IEEE Sensors Journal **13**(12), 2013: 4808-4816. https://doi.org/10.1109/JSEN.2013.2274008
[15] Al-Tarawneh M., Huang Y., *In-pavement fiber Bragg grating sensor for vehicle speed and wheel-base estimation*, Proceedings of the SPIE, Vol. 10598, Sensors and Smart Structures Technologies for Civil, Mechanical, and Aerospace Systems 2018: 105982A. https://doi.org/10.1117/12.2295624
[16] Al-Tarawneh M., Huang Y., Lu P., Tolliver D., *Vehicle classification system using in-pavement fiber Bragg grating sensors*, IEEE Sensors Journal **18**(7), 2018: 2807-2815. https://doi.org/10.1109/JSEN.2018.2803618
[17] Zhang Z., Huang Y., Bridgelall R., Palek L., Strommen R., *Sampling optimization for high-speed weigh-in-motion measurements using in-pavement strain-based sensors*, Measurement Science and Technology **26**(6), 2015: 065003. https://doi.org/10.1088/0957-0233/26/6/065003
[18] Liu Z., Shao T., Zhang X., *BCG signal analysis based on improved VMD algorithm*, Measurement **231**, 2024: 114631. https://doi.org/10.1016/j.measurement.2024.114631
[19] Shao T.P., Liu Z.C., *Design of pulse and respiration monitoring system based on fiber optic sensing and VMD-FPR processing algorithm*, Optical Fiber Technology **73**, 2022: 103033. https://doi.org/10.1016/j.yofte.2022.103033
[20] Liu Z.C., Zhang X., Shao T.P., Meng J.H., *Heartbeat and respiration monitoring based on FBG sensor network*, Optical Fiber Technology **81**, 2023: 103561. https://doi.org/10.1016/j.yofte.2023.103561
[21] De Fazio R., Greco M.R., De Vittorio M., Visconti P., *A differential inertial wearable device for breathing parameter detection: Hardware and firmware development, experimental characterization*, Sensors **22**(24), 2022: 9953. https://doi.org/10.3390/s22249953

Received September 24, 2024
in revised form November 18, 2024